AGU100 ADVANCING EARTH AND SPACE SCIENCE

Geophysical Research Letters

RESEARCH LETTER
10.1029/2019GL083452

Key Points:
- Precipitation extent and intensity vary strongly among categories of tropical cyclones
- The largest extents and heaviest intensities of overall rainfall over land occur for major hurricanes that have weakened to tropical storms
- Heavy precipitation has significantly increased between 1900–1957 and 1958–2017 for major hurricanes that have weakened to tropical storms

Supporting Information:
- Supporting Information S1

Correspondence to:
D. Touma,
touma@ucsb.edu

Citation:
Touma, D., Stevenson, S., Camargo, S. J., Horton, D. E., & Diffenbaugh, N. S. (2019). Variations in the intensity and spatial extent of tropical cyclone precipitation. *Geophysical Research Letters*, *46*, 13,992–14,002. https://doi.org/10.1029/2019GL083452

Received 24 APR 2019
Accepted 8 OCT 2019
Accepted article online 18 OCT 2019
Published online 4 DEC 2019

Variations in the Intensity and Spatial Extent of Tropical Cyclone Precipitation

Danielle Touma[1,2], Samantha Stevenson[1], Suzana J. Camargo[3], Daniel E. Horton[4], and Noah S. Diffenbaugh[2,5]

[1]Bren School of Environmental Science & Management, University of California, Santa Barbara, CA, USA, [2]Department of Earth System Science, Stanford University, Stanford, CA, USA, [3]Lamont-Doherty Earth Observatory, Columbia University, Palisades, NY, USA, [4]Department of Earth and Planetary Sciences, Northwestern University, Evanston, IL, USA, [5]Woods Institute for the Environment, Stanford University, Stanford, CA, USA

Abstract The intensity and spatial extent of tropical cyclone precipitation (TCP) often shapes the risk posed by landfalling storms. Here we provide a comprehensive climatology of landfalling TCP characteristics as a function of tropical cyclone strength, using daily precipitation station data and Atlantic U.S. landfalling tropical cyclone tracks from 1900 to 2017. We analyze the intensity and spatial extent of ≥1 mm/day TCP (Z_1) and ≥50 mm/day TCP (Z_{50}) over land. We show that the highest median intensity and largest median spatial extent of Z_1 and Z_{50} occur for major hurricanes that have weakened to tropical storms, indicating greater flood risk despite weaker wind speeds. We also find some signs of TCP change in recent decades. In particular, for major hurricanes that have weakened to tropical storms, Z_{50} intensity has significantly increased, indicating possible increases in flood risk to coastal communities in more recent years.

Plain Language Summary Heavy and widespread rainfall during landfalling tropical cyclones can cause severe damage and large financial losses. Here we investigate the differences in rainfall along tracks of tropical cyclones of different intensities. To do this, we examine the tracks of Atlantic tropical cyclones that made landfall in the southeastern and eastern United States during the 20th century. Across all major hurricanes, the largest areas and heaviest intensities of rainfall over land occur after they have weakened to tropical storms. These major hurricanes that have weakened to tropical storms also have heavier rainfall over land during the most recent six decades compared to the first six decades of our study period. Our findings indicate that after landfall occurs, the greatest risks of heavy and widespread rainfall are associated with major hurricanes that have weakened to tropical storms and that these risks may have grown in the past century.

1. Introduction

Tropical cyclones have contributed to thousands of fatalities and billions of dollars in losses in the United States in recent years. This includes more than 3,000 deaths and $300B in financial losses from hurricanes Michael, Florence, Harvey, Irma, and Maria in 2017 and 2018 (NOAA, 2019). Coastal and inland flooding due to heavy tropical cyclone precipitation (TCP) can have extensive impacts on human health (Bell et al., 2018), including 27% of fatalities during tropical cyclones between 1963 and 2012 (Rappaport, 2000, 2013). Extreme TCP can drastically increase a storm's impacts. For example, Hurricane Harvey's (2017) vast and heavy rainfall contributed to 57 of the 70 deaths and $11B of losses due to multiday flooding (Jonkman et al., 2018; Simpson, 2018), and the majority of Tropical Storm Allison's (2001) damages, including 41 deaths and $5B in losses, were due to heavy, prolonged, and widespread rainfall (Beven et al., 2002; National Centers for Environmental Prediction, 2001). These examples highlight the multiplicative damage that high-magnitude and large-footprint TCP can yield. Such impacts are particularly acute when flooding occurs in several metropolitan areas simultaneously, significantly impeding evacuation, relief, and recovery efforts (Upton et al., 2017; Yeo et al., 2018).

The impacts of recent storms provide ample motivation to better understand the factors that shape TCP intensity and spatial extent, which often vary drastically among tropical cyclones (Matyas, 2010; Skok et al., 2013). Multiple studies have examined the relationship between TCP and TC intensity over the

Atlantic region (e.g., Chen et al. (2006), Daloz et al. (2010), Gaona and Villarini (2018), Jiang et al. (2008), Konrad and Perry (2009), Lau and Zhou (2012), Prat and Nelson (2016), Zhou and Matyas (2017) and Zick and Matyas (2016)). Using radar, satellite, or station observations, these studies conclude that TCs that make landfall as major or minor hurricanes (as opposed to tropical storms) deliver the highest TCP rates and accumulations of TCP as they weaken over land. Additionally, as a TC makes landfall, TCP intensity increases in the outer bands of the storm (Villarini et al., 2011), and storm structures become more asymmetric and fragmented (Zhou & Matyas, 2017; Zick & Matyas, 2016). These studies highlight the importance of understanding the risks associated with TCP as a function of TC evolution.

While previous studies assessed TCP differences among landfalling TC intensity categories, most are limited to relatively short satellite or radar records, and few discriminate between TC intensity categories *after* landfall. Given the precipitation-related risks posed by TCs as they travel inland, our study aims to identify how climatological TCP intensity and spatial extent over land differ for different maximum and transitional TC intensities during the 20th century. Using the geostatistical framework described in Touma et al. (2018), we quantify the spatial extent of TCP directly from meteorological stations. The use of station data eliminates the need to interpolate or smooth precipitation observations, which can limit the accuracy of TCP quantification (Villarini et al., 2011). Additionally, station observations allow us to overcome the temporal limitations of satellite and radar records, enabling TCP quantification from the beginning of the 20th century to the present, the longest period analyzed to date.

We systematically investigate TCP characteristics and trends as a function of TC intensity. Our study also aims to shed light on variations in TCP intensity and spatial extent during and after landfall, as TCs travel inland and weaken. Given that both the intensity and spatial extent of TCP can modify the impacts to affected regions, but do not always vary congruously (e.g., Patricola and Wehner (2018) and Villarini et al. (2011)), we separately quantify variations in both the intensity and spatial extent. Moreover, we assess variations in lighter and heavier thresholds of TCP over land to understand the added risks from higher levels of TCP.

Analyzing the period since the beginning of the 20th century captures a larger range of TCP variability than in previous studies and allows us to test whether there have been changes in TCP intensity and/or spatial extent through time. This analysis is motivated by previous work showing a role for global warming in altering large-scale atmospheric conditions (Ross & Elliot, 1996; Trenberth et al., 2005), atmospheric moisture availability (Allan & Soden, 2008; Held & Soden, 2006), and tropical cyclone characteristics (Knutson et al., 2010; Sobel et al., 2016; Walsh et al., 2016). Previous observational analyses of TCP trends yield somewhat contradictory conclusions (Dhakal & Tharu, 2018; Knutson et al., 2018; Kunkel et al., 2010; Zhu & Quiring, 2013), yet modeling results suggest that mean and extreme TCP will increase with anthropogenic climate change (Knutson et al., 2010; Liu et al., 2018; Villarini et al., 2014). Additionally, previous studies have used global- and regional-scale models to attribute unprecedented intensities of TCP, such as during Hurricane Harvey (2017), to observe anthropogenic warming and have projected future increases in TCP under continued global warming (Emanuel, 2017; Patricola & Wehner, 2018; Risser & Wehner, 2017; van Oldenborgh et al., 2017; Wang et al., 2018). Extending the observational baseline of TCP estimates over the past century is thus crucial for constraining future projections.

2. Data and Methods

2.1. Station Precipitation and Tropical Cyclone Tracks

We use daily precipitation data from the Global Historical Climatology Network (GHCN)-Daily station data set (Menne et al., 2012) and TC tracks archived in the revised HURricane DATabase (HURDAT2) database (Landsea & Franklin, 2013). HURDAT2 is a poststorm reanalysis that uses several data sets, including land observations, aircraft reconnaissance, ship logs, radiosondes, and satellite observations to determine tropical cyclone track locations, wind speeds, and central pressures (Jarvinen et al., 1984; Landsea & Franklin, 2013). We select 1,256 U.S. stations from the GHCN-Daily data set that have observations beginning no later than 1900 and ending no earlier than 2017 (though most station records are not continuous throughout that period). These 1,256 land-based stations are well distributed over the southeastern United States and Atlantic seaboard (see Supporting Information Figure S1).

We use the HURDAT2 Atlantic database to select locations and windspeeds of TC tracks that originated in the North Atlantic Ocean, Gulf of Mexico, and Caribbean Sea and made landfall over the continental United States. Though tracks are determined at 6-hourly time steps for each storm (with additional time steps that indicate times of landfall and times and values of maximum intensity), we limit our analysis to track points recorded at 1200 UTC, in order to match the daily temporal resolution and times of observation of the GHCN-Daily precipitation data set (Menne et al., 2012), as well as the diurnal cycle of TCP (Gaona & Villarini, 2018). Although this temporal matching technique may omit high values of precipitation from the analysis, it reduces the possibility of capturing precipitation that is not associated with a TC.

2.2. Tropical Cyclone and Lifetime Maximum Intensity Categories

For each daily point in the tropical cyclone track, we use the maximum sustained windspeed to place the storm into one of three Extended Saffir-Simpson categories: tropical storms ("TS"; 34–63 knots), minor hurricanes ("Min"; categories 1 and 2; 64–95 knots), and major hurricanes ("Maj"; categories 3 to 5; >96 knots; Schott et al., 2012). Additionally, for each track, we record the category of the lifetime maximum intensity (LMI), based on the maximum windspeed found along the whole lifetime of the track (i.e., using all available track points). LMI is a standard tropical cyclone metric and is considered a robust measure of track intensity through time and across different types of data integrated into the HURDAT2 reanalysis (Elsner et al., 2008; Kossin et al., 2013, 2014). Therefore, for each track point, a dual category is assigned: the first portion of the classification denotes the category of the storm for a given point (hereafter "point category"), while the second denotes the LMI category. The combination of the two can thus be considered a "point-LMI category." For example, the point on 27 August 2017 at 1200 UTC along Hurricane Harvey's track is classified as TS-Maj because it is a tropical storm (TS) at this point but falls along a major hurricane LMI track (see starred location in Figure S2a). Given that the LMI category for a given point cannot be weaker than the point category itself, the set of possible point-LMI category combinations for each track point is TS-TS, TS-Min, TS-Maj, Min-Min, Min-Maj, and Maj-Maj. This dual classification allows us to explore climatological TCP spatial extents and intensities during the tropical cyclone lifetime. Our dual classification does not account for the timing of the point category relative to the LMI category for a given point along a track (i.e., the time lag between the LMI and point in consideration). However, the majority of points selected in our analysis occur after the TC has reached its LMI and are in the weakening stage (see Table S1 for more details). This could be expected, as our analysis is focused on land-based precipitation stations, and TCs weaken over land. However, a small fraction of TC points analyzed occur over the ocean before making landfall but are close enough to land for precipitation gauges to be impacted.

2.3. Moving Neighborhood Method for TCP Spatial Extent and Intensity

We first find the distribution of TCP intensity using all daily land precipitation values from all available stations in a 700-km-radius neighborhood around each point over land on each tropical cyclone track (Figures 1a and S2). We then create two new binary station data sets, $Z_1(x)$ and $Z_{50}(x)$, which indicate whether or not a station meets or exceeds the 1 or 50 mm/day precipitation threshold, respectively, on a given day. The 50 mm/day threshold is greater than the 75th percentile of TCP across all tropical cyclone categories (Figure 1a), allowing us to capture the characteristics of heavy TCP while retaining a robust sample size. The 1 mm/day threshold captures the extent of the overall TCP around the TC track point.

We use the relaxed moving neighborhood and semivariogram framework developed by Touma et al. (2018) to quantify the spatial extent of Z_1 and Z_{50} TCP for each track point. Using a neighborhood with a 700-km radius around each track point, we select all station pairs that meet two criteria: at least one station has to exhibit the threshold precipitation on that given day ($Z(x) = 1$; blue and pink stations in Figure S2b) and at least one station has to be inside the neighborhood (black and pink stations in Figure S2b). We then calculate the indicator semivariogram, $\gamma(h)$, for each station pair selected for that track point (equation (1)):

$$\gamma(h) = \frac{1}{2}[Z(x+h) - Z(x)]^2, \tag{1}$$

where h is the separation distance between the stations in the station pair. The indicator semivariogram is a function of the separation distance and has two possible outcomes: all pairs with two threshold stations ($Z(x) = Z(x+h) = 1$) have a semivariogram value of 0, and all pairs with one threshold station and one non-threshold station ($Z(x) = 1$ and $Z(x+h) = 0$) have a semivariogram value of 0.5.

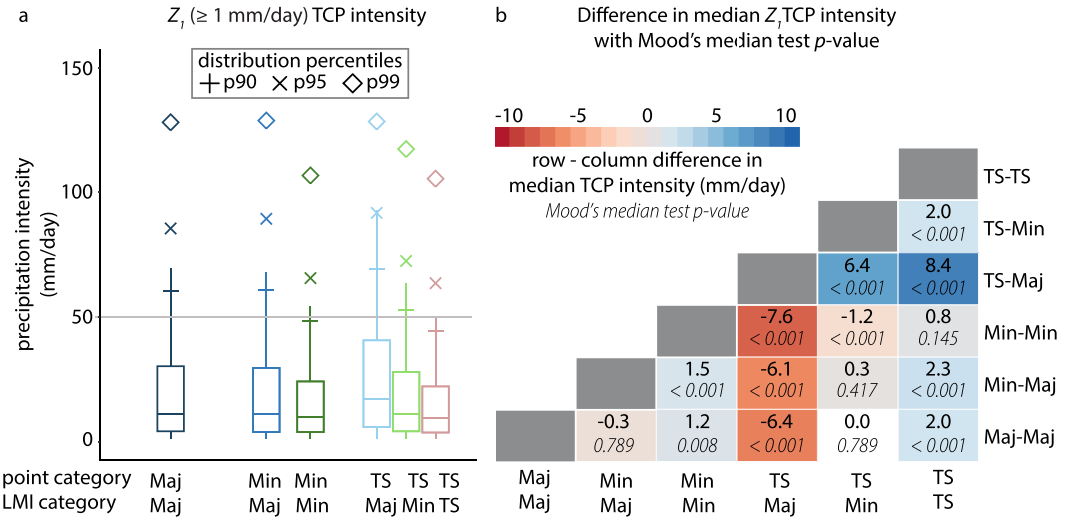

Figure 1. (a) The distribution of Z_1 TCP intensity for each point-LMI category. The 90th, 95th, and 99th percentiles of the distributions are indicated by the symbols. (b) The differences in Z_1 TCP intensity among the different point-LMI classifications are shown as bold numbers and shading. The number and shading of each grid represents the difference of the median TCP intensity of the row category minus the column category. The adjusted *p* values of Mood's median test when comparing the distributions among the categories are shown in italics. LMI = lifetime maximum intensity; TCP = tropical cyclone precipitation.

We then average the semivariogram values for all station pairs for equal intervals of separation distances (up to 1,000 km) to obtain the experimental semivariogram (Figure S2c). To quantify the shape of the experimental semivariogram, we fit three parameters of the theoretical spherical variogram (nugget, partial sill, and practical range) to the experimental semivariogram (equation (2)):

$$\gamma h = \begin{cases} 0, & h = 0 \\ c + b\dfrac{3h}{2\alpha} - \dfrac{1h^3}{2\alpha}, & 0 < h \le \alpha \\ c + b, & h \ge \alpha \end{cases} \quad (2)$$

where c is the nugget, b is the partial sill, and α is the practical range (Goovaerts, 2015). The nugget quantifies measurement errors or microscale variability, and the partial sill is the maximum value reached by the spherical semivariogram (Goovaerts, 2015). The practical range is the separation distance at which the semivariogram asymptotes (Figure S2c). At this separation distance, station pairs are no longer likely to exhibit the threshold precipitation (1 or 50 mm/day) simultaneously (Goovaerts, 2015; Touma et al., 2018). Therefore, as in Touma et al. (2018), we define the length scale—or spatial extent—of TCP for that given track point as the practical range.

There are some subjective choices of the moving neighborhood and semivariogram framework, including the 700-km radius of neighborhood (Touma et al., 2018). Previous studies found that 700 km is sufficient to capture the extent to which tropical cyclones influence precipitation (e.g., Barlow (2011), Daloz et al. (2010), Hernández Ayala and Matyas (2016), Kim et al. (2014), Knaff et al. (2014), Knutson et al. (2010) and Matyas (2010)). Additionally, Touma et al. (2018) showed that although the neighborhood size can slightly impact the magnitude of length scales, it has little impact on their relative spatial and temporal variations.

2.4. Analysis of Variations and Trends

We use Mood's median test (Desu & Raghavarao, 2003) to test for differences in the median TCP intensity and spatial extent among point-LMI categories, adjusting *p* values to account for multiple simultaneous comparisons (Benjamini & Hochberg, 1995; Holm, 1979; Sheskin, 2003). To test for changes in TCP characteristics over time, we divide our century-scale data set into two halves, 1900–1957 and 1958–2017. First, the

quartile boundaries are established using the distributions of the earlier period (1900–1957), with one quarter of the distribution falling in each quartile. Then, we find the fraction of points in each quartile in the later period (1958–2017) to determine changes in the distribution. We also report the p values of the Kolmogorov-Smirnov test to quantify the differences in the full distributions of TCP intensity and extent between the earlier and later periods (Sheskin, 2003; see Text S1 for more details). Further, to determine the effect of multi-annual variability on the changes between the earlier and later periods of our data set, we calculate changes in TCP intensity and extent using midpoint years ranging from 1947 to 1967.

3. Results

3.1. Climatology of TCP Intensity and Spatial Extent

Our systematic, century-scale analysis reveals significant differences in TCP characteristics among point-LMI categories. Tropical storms that reach major hurricane intensity at some point along their track (TS-Maj) have larger median precipitation intensity than all other point-LMI categories (Min-Maj, Maj-Maj, TS-Min, Min-Min, and TS-TS; Figure 1). While major hurricane LMI tracks have higher median TCP intensity than minor hurricane and tropical storm LMI tracks ($p < 0.001$; Figure S3), the median TCP intensity for TS-Maj track points exceeds the median for Min-Maj track points by 6.1 mm/day ($p < 0.001$) and Maj-Maj track points by 6.4 mm/day ($p < 0.001$; Figure 1b). Similarly, of those tropical cyclones that reach minor hurricane intensity (TS-Min and Min-Min), the largest median TCP intensity also occurs when they weaken to tropical storms (TS-Min; $p < 0.001$; Figure 1b). TS-Maj, Min-Maj, and Maj-Maj show the highest TCP values in the upper tails of the distributions (Figure 1a). In these categories, the 90th percentile is 60 mm/day, compared with 45 mm/day for the set of all categories. While previous studies have noted that the highest TCP intensities are found along major and minor hurricane tracks (Konrad & Perry, 2009; Lau & Zhou, 2012), we show that, for the portion of the tracks that occur over land, these high TCP intensities occur during their weaker TS phases (TS-Maj and TS-Min). In contrast, tropical storms that never reach hurricane intensity (TS-TS) have the lowest median TCP intensity of all categories (Figure 1b).

We next consider variations in TCP extent. Z_1 and Z_{50} median extents are larger along major hurricane LMI tracks than along minor hurricane and tropical storm LMI tracks (Figures S3d and S3e). However, we find that the median Z_1 extent for TS-Maj events is 163 km larger than Min-Maj events ($p = 0.002$) and 232 km larger than Maj-Maj events ($p = 0.007$; Figure 2a). While the differences are not as robust, the median Z_{50} extent of TS-Maj events is also larger than the Min-Maj and Maj-Maj portions of major hurricane tracks (Figure 2b). Similarly, median TS-Min Z_1 and Z_{50} extents are 98 km ($p = 0.002$) and 24 km ($p = 0.311$) larger, respectively, than the median Min-Min extents (Figure 2). Therefore, landfalling TCs that have at some point reached major or minor hurricane intensity are more likely to be associated with larger median TCP extents and intensities over land after they have weakened to tropical storms.

3.2. Changes in TCP Intensity and Spatial Extent

Global ocean and atmosphere temperatures have warmed since the beginning of the 20th century (Hansen et al., 2010; Hartmann et al., 2013; Lenssen et al., 2019; Team, 2019; Vose et al., 2012). Therefore, any responses of TCP to anthropogenic warming could possibly be detected between the earlier and later halves of our century-scale data sets. We find strong changes in Z_1 TCP intensity distributions for the strongest intensities of major hurricanes (Maj-Maj) and during their weakened tropical storm intensities (TS-Maj; $p < 0.001$; Figure 3c). For both TS-Maj and Maj-Maj, there has been a negative shift in Z_1 TCP intensity distributions in 1958–2017 relative to 1900–1957 (Figure 3c). However, 14% of the points in the Z_{50} TCP intensity distributions of TS-Maj have shifted toward the upper quartiles in the later period, with high (>70 mm/day) values becoming more common, and significantly changing the distribution of Z_{50} TCP intensity ($p < 0.001$; Figures 3a and 3b). Thus, risks due to heavy Z_{50} TCP may have increased in the second half of the century for major hurricanes; but this increase is most robust for those that have weakened to tropical storms.

We next consider changes in the spatial extent of TCP. The distributions of Z_1 extent for the weakest phases of major hurricanes (TS-Maj) are significantly different between the earlier and later periods ($p = 0.048$; Figure 3e); 24% of the points in the Z_1 TCP extent distribution have shifted from the upper two quartiles to the lower quartiles (Figure 3e). We note that there is a lack of statistically significant changes in the Z_1

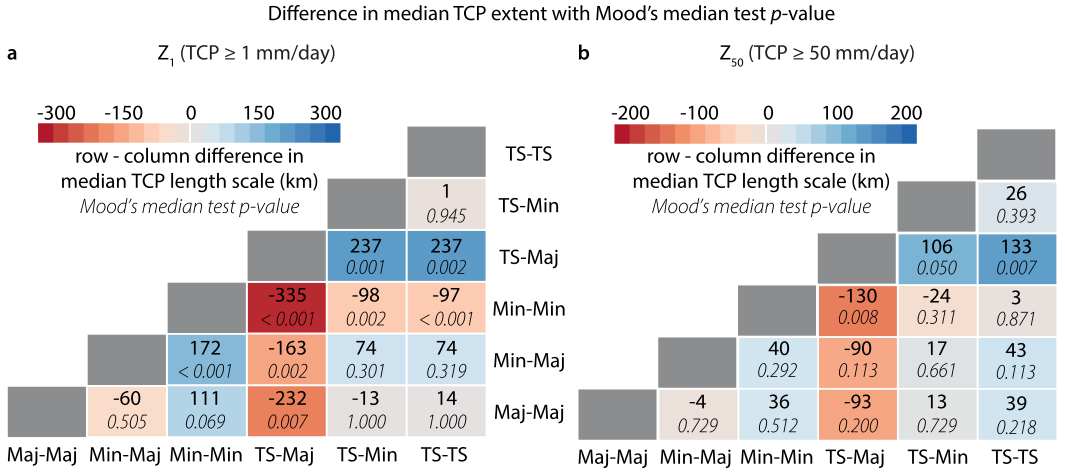

Figure 2. The differences in Z_1 (a) and Z_{50} (b) TCP extents among the different point-LMI classifications. The number and shading of each grid represents the difference of the median TCP extent of the row category minus the column category. The adjusted p values of Mood's median test when comparing the medians among the categories are shown in italics. LMI = lifetime maximum intensity; TCP = tropical cyclone precipitation.

extent distributions for the strongest phases of major hurricanes (Maj-Maj and Min-Maj) and no significant changes in the Z_{50} extent distributions (Figures 3d and 3e). However, the shift toward the lower quartile in the distributions of TS-Maj Z_1 TCP extent suggests a diminished spatial extent of TCP around the tropical cyclone track over land during the weakest phases of major hurricanes.

The well-documented interannual and decadal variability in Atlantic tropical cyclone activity has been tied to the El Niño–Southern Oscillation, Atlantic Multidecadal Oscillation, and Atlantic Meridional Mode, as well as other modes of variability (Boudreault et al., 2017; Camargo et al., 2007; Goldenberg, 2001; Gray, 1984; Hall & Hereid, 2015; Hart et al., 2016; Klotzbach et al., 2018; Knutson et al., 2010; Kossin & Vimont, 2007; Patricola et al., 2014; Truchelut & Staehling, 2017). Thus, the changes in TCP intensity and extent may be sensitive to the "cutoff" year used as the midpoint between our two periods. However, we find that most changes remain intact when using different cutoff years (see Figures S5 and S6). For example, the increases in the upper quartiles of the Z_{50} TCP intensity for TS-Maj points are robust across all cutoff years (see Figure S5f). An explicit analysis of the relationship between TCP characteristics and the multiannual modes of variability (similar to Khouakhi et al. (2017)) will allow us to further distinguish background variability from historical changes in TCP.

4. Discussion and Conclusions

Our quantification of climatological intensity and extents of landfalling TCP has implications for assessment of the hazards associated with different tropical cyclone intensities. We find that the most intense and widespread TCP occurs for tropical cyclones that have a major hurricane LMI (see Figure S3) and that the greatest median TCP extents and intensities occur after these storms have reached their strongest intensity and weakened to tropical storms (Figures 1 and 2). Although previous studies have diagnosed the expansion and intensification of TCP in landfalling tropical cyclones (Blackwell, 2000; Dong et al., 2010; Liu & Smith, 2016; Matyas, 2010; Villarini et al., 2011; Yu & Cheng, 2013; Zhou & Matyas, 2017; Zhu & Quiring, 2013; Zick & Matyas, 2016), our study reveals that major hurricanes have significantly larger spatial extents of overall TCP over land once they have weakened to tropical storms. Understanding the tropical storm portion of a major hurricane's evolution appears to be key to managing the risks posed by major hurricanes as they travel inland and weaken to tropical storms, bringing heavier TCP along their tracks.

While the use of a century-scale daily precipitation data set allows insight into the long-term climatology of TCP variations, it prevents the analysis of instantaneous, or subdaily, TCP. For example, our daily precipitation totals do not explicitly differentiate between high values of TCP intensity caused by a slow-moving TC with lighter TCP rates versus a fast-moving TC with heavier TCP rates. The causes for such differences in the

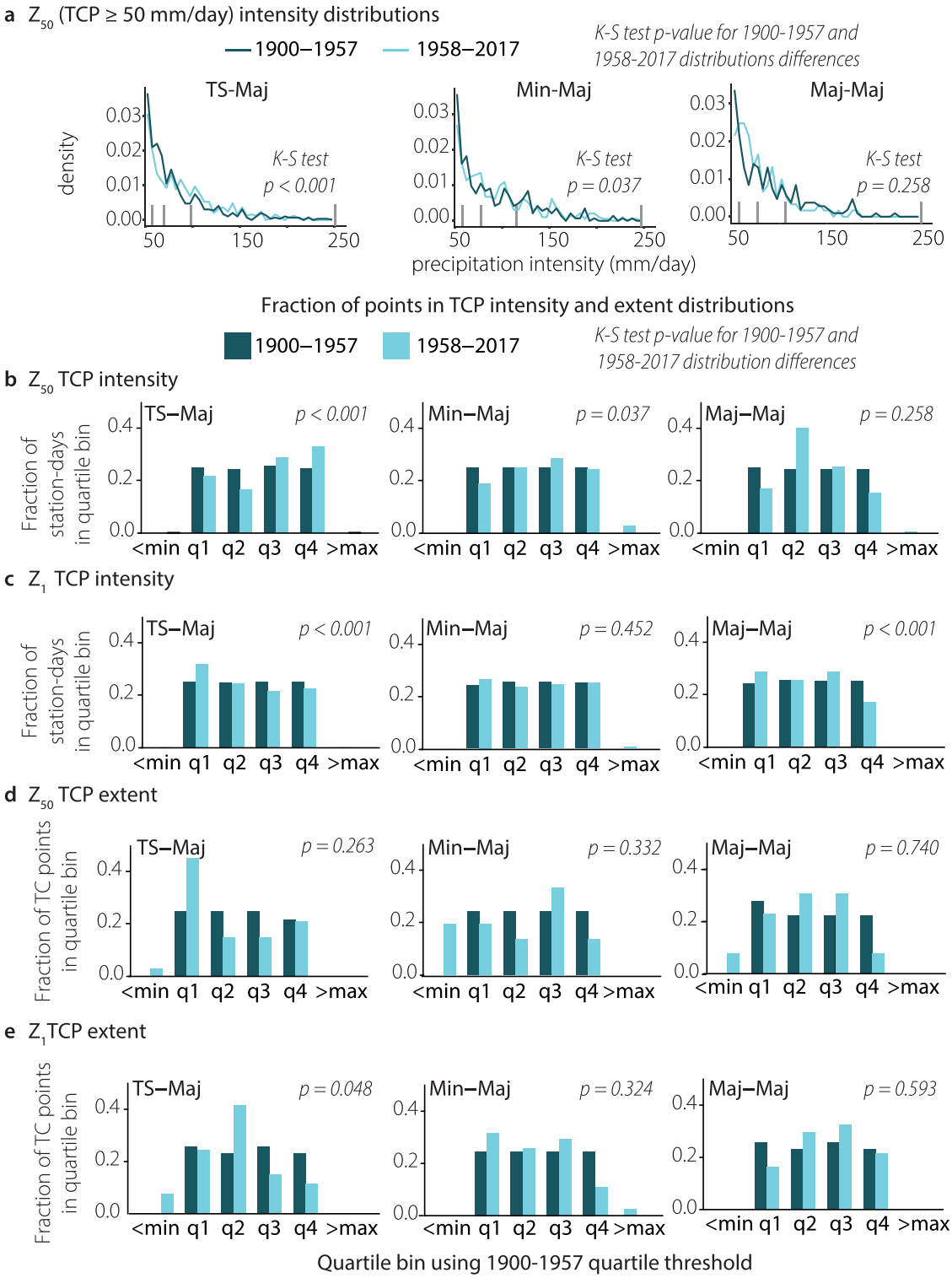

Figure 3. (a) Frequency distributions for Z_{50} TCP intensity for TS-Maj (left), Min-Maj (middle), and Maj-Maj (right) point-LMI categories for 1900–1957 (dark teal) and 1958–2017 (light teal). The short vertical gray lines mark quartile boundaries in the earlier period. (b, c, d, e) Fraction of points in each quartile bin of the distribution for the earlier (1900–1957) and later periods (1958–2017), where the quartile thresholds are established using the earlier period (1900–1957) distribution for Z_{50} TCP intensity (b), Z_1 TCP intensity (c), Z_{50} TCP extent (d), and Z_1 TCP extent (e). The p value of the Kolmogorov-Smirnov (K-S) test for the distributions in the earlier and the later periods is shown in italics in panels (a), (b), (c), (d), and (e). (Fraction of points in the earlier period are not always exactly equal to 0.25 because the fraction of points are recalculated using the number of points that are in each bin, and the sample sizes do not always divisible by four.) TCP = tropical cyclone precipitation.

accumulation of daily TCP among tropical cyclone categories could potentially be diagnosed by assessing the translation speed of TC tracks. We find that for all tropical storms (TS-TS, TS-Min, and TS-Maj), those along major hurricane LMI tracks (TS-Maj) have the fastest median translation speed (see Figure S7). Therefore, the relatively high daily TCP intensity values during the tropical storm phases of major hurricanes (Figure 1) are more likely a result of relatively high subdaily rates of rainfall, rather than sustained accumulation due to slower translation speeds. While high subdaily rates of rainfall during landfalling major hurricanes have been quantified in previous studies using short-term satellite and radar data (e.g., Gaona et al. (2018), Gaona and Villarini (2018) and Villarini et al. (2011)), a higher temporal resolution of station-based precipitation observations would be advantageous to illuminate the potential role of tropical cyclone dynamics in shaping TCP characteristics.

Our results also show increases in the upper half of the Z_{50} TCP intensity distribution for tropical storms along major hurricane tracks (TS-Maj) in 1958–2017 compared to 1900–1957 (Figures 3a and 3b). This indicates that the strongest increase in TCP risk over our analysis period has occurred for major hurricanes that weaken to tropical storms over land. These positive shifts in high values of TCP intensity for tropical storms and minor hurricanes that were once major hurricanes can be plausibly linked to higher amounts of precipitable water in a warmer atmosphere, as demonstrated in previous studies (Emanuel, 2017; Patricola & Wehner, 2018; Ross & Elliot, 1996; Scoccimarro et al., 2014; Trenberth et al., 2003, 2005; Villarini et al., 2013; Wang et al., 2018). We also find some indication that the largest overall TCP spatial extents for major hurricanes that have weakened to tropical storms have decreased throughout the century, indicating the potential for more localized impacts of TCP and highlighting the importance of improving TC track forecasts for major hurricanes while they weaken over land. While this decrease in TCP extent has yet to be shown in other observational studies, modeling studies show decreases in the areal extent of TCP under warmer atmospheric conditions (Patricola & Wehner, 2018). Given that these modeling studies are limited to a small number of hurricanes, and only show TCP composites over the full track (over both the ocean and land), a direct comparison of their findings with ours would require additional modeling and analysis. Further investigation is also needed to understand why strong changes in TCP extent are only found for major hurricanes that have weakened to tropical storms.

Our century-scale empirical study could help to inform flood preparedness and risk management by specifically partitioning changes in TCP characteristics between different intensities of tropical cyclones at landfall. While several studies have used climate models to assess potential changes in TCP under warmer conditions (Emanuel, 2017; Kim et al., 2014; Knutson et al., 2013; Patricola & Wehner, 2018; Wright et al., 2015) and altered land use (Zhang et al., 2018), our study adds key observational context for interpreting projected changes of TCP intensity and extents. Climate model projections suggest that a larger proportion of tropical cyclones could intensify to major hurricanes over the ocean in response to warmer sea surface temperatures (Kim et al., 2014; Knutson et al., 2013; Sobel et al., 2016). Our results suggest that as these major hurricanes make landfall, their *weakening* intensities could potentially have an increased likelihood of more localized, higher TCP intensities, amplifying the potential for flood devastation such as witnessed during events like hurricanes Harvey and Florence.

Acknowledgments
We thank two anonymous reviewers for their valuable feedback and suggestions. This research was funded in part by the Department of Energy and Stanford University. S. J. C. acknowledges partial funding from the National Oceanographic and Atmospheric Administration (NOAA) Grants NA15OAR4310095, NA16OAR4310079, and NA18OAR4310277. S. S. is supported by US Department of Energy Grant DE-SC0019418. We thank the Stanford Research Computing Center for providing computational resources and support that contributed to these research results. We thank National Oceanographic and Atmospheric Administration (NOAA) for providing the Global Historical Climatology Network (GHCN) station data and NOAA's National Hurricane Center (NHC) for providing the best track data from the revised HURricane DATabase (HURDAT2) data set. The GHCN-Daily station data is available from NOAA (https://www.ncdc.noaa.gov/ghcnd-data-access) and the HURDAT2 data set is available from NOAA NHC (https://www.aoml.noaa.gov/hrd/hurdat/Data_Storm.html). We thank the University of California, Santa Barbara Library for hosting the data shown in this paper. Data that were processed by authors following the Methods and subsequently presented in the manuscript and Supporting Information can be found at the following DOI: https://doi.org/10.25349/D9F30M.

References

Allan, R. P., & Soden, B. J. (2008). Atmospheric warming and the amplification of precipitation extremes. *Science*, *321*(5895), 1481–1484. https://doi.org/10.1126/science.1160787

Barlow, M. (2011). Influence of hurricane-related activity on North American extreme precipitation. *Geophysical Research Letters*, *38*, L04705. https://doi.org/10.1029/2010GL046258

Bell, J. E., Brown, C. L., Conlon, K., Herring, S., Kunkel, K. E., Lawrimore, J., et al. (2018). Changes in extreme events and the potential impacts on human health. *Journal of the Air and Waste Management Association*, *68*(4), 265–287. https://doi.org/10.1080/10962247.2017.1401017

Benjamini, Y., & Hochberg, Y. (1995). Controlling the false discovery rate: A practical and powerful approach to multiple testing. *Journal of the Royal Statistical Society: Series B (Methodological)*, *57*(1), 289–300. https://doi.org/10.1111/j.2517-6161.1995.tb02031.x

Beven, J. L., Stewart, S. R., Lawrence, M. B., Avila, L. A., Franklin, J. L., & Pasch, R. J. (2002). Atlantic hurricane season of 1972. *Monthly Weather Review*, *131*, 1454–1484.

Blackwell, K. G. (2000). The evolution of Hurricane Danny (1997) at landfall: Doppler-observed eyewall replacement, vortex contraction/intensification, and low-level wind maxima. *Monthly Weather Review*, *128*(12), 4002–4016. https://doi.org/10.1175/1520-0493(2000)129<4002:TEOHDA>2.0.CO;2

Boudreault, M., Caron, L. P., & Camargo, S. J. (2017). Reanalysis of climate influences on Atlantic tropical cyclone activity using cluster analysis. *Journal of Geophysical Research: Atmospheres*, *122*, 4258–4280. https://doi.org/10.1002/2016JD026103

Camargo, S. J., Emanuel, K. A., & Sobel, A. H. (2007). Use of a genesis potential index to diagnose ENSO effects on tropical cyclone genesis. *Journal of Climate*, *20*(19), 4819–4834. https://doi.org/10.1175/JCLI4282.1

Chen, S. S., Knaff, J. A., & Marks, F. D. (2006). Effects of vertical wind shear and storm motion on tropical cyclone rainfall asymmetries deduced from TRMM. *Monthly Weather Review*, *134*(11), 3190–3208. https://doi.org/10.1175/MWR3245.1

Daloz, A. S., Chauvin, F., & Roux, F. (2010). Tropical cyclone rainfall in the observations, reanalysis and ARPEGE simulations in the North Atlantic Basin. In J. B. Elsner, R. E. Hodges, J. C. Malmstadt, & K. N. Scheitlin (Eds.), *Hurricanes and climate change* (Vol. 3, pp. 57–79). Dordrecht, Netherlands: Springer. https://doi.org/10.1007/978-90-481-9510-7_4

Desu, M. M., & Raghavarao, D. (2003). *Nonparametric statistical methods for complete and censored data*. New York: Chapman and Hall/CRC. https://doi.org/10.1201/9781482285895

Dhakal, N., & Tharu, B. (2018). Spatio-temporal trends in daily precipitation extremes and their connection with North Atlantic tropical cyclones for the southeastern United States. *International Journal of Climatology*, *38*(10), 3822–3831. https://doi.org/10.1002/joc.5535

Dong, M., Chen, L., Li, Y., & Lu, C. (2010). Rainfall reinforcement associated with landfalling tropical cyclones. *Journal of the Atmospheric Sciences*, *67*(11), 3541–3558. https://doi.org/10.1175/2010JAS3268.1

Elsner, J. B., Kossin, J. P., & Jagger, T. H. (2008). The increasing intensity of the strongest tropical cyclones. *Nature*, *455*(7209), 92–95. https://doi.org/10.1038/nature07234

Emanuel, K. (2017). Assessing the present and future probability of Hurricane Harvey's rainfall. *Proceedings of the National Academy of Sciences*, *114*(48), 12,681–12,684. https://doi.org/10.1073/pnas.1716222114

Gaona, M. F. R., & Villarini, G. (2018). Characterization of the diurnal cycle of maximum rainfall in tropical cyclones. *Journal of Hydrology*, *564*(December 2017), 997–1007. https://doi.org/10.1016/j.jhydrol.2018.07.062

Gaona, M. F. R., Villarini, G., Zhang, W., & Vecchi, G. A. (2018). The added value of IMERG in characterizing rainfall in tropical cyclones. *Atmospheric Research*, *209*(March), 95–102. https://doi.org/10.1016/j.atmosres.2018.03.008

Goldenberg, S. B. (2001). Causes and implications the recent increase in Atlantic hurricane activity: Causes and implications. *Science*, *293*(5529), 474–479. https://doi.org/10.1109/ICCSIT.2009.5234572

Goovaerts, P. (2015). Geostatistical analysis of spatial data. Geoinformatics.

Gray, W. M. (1984). Atlantic seasonal hurricane frequency. Part I: El Niño and 30 mb quasi-biennial oscillation influences. *Monthly Weather Review*, *112*(9), 1649–1668. https://doi.org/10.1175/1520-0493(1984)112<1649:ASHFPI>2.0.CO;2

Hall, T., & Hereid, K. (2015). The frequency and duration of US hurricane droughts. *Geophysical Research Letters*, *42*, 3482–3485. https://doi.org/10.1002/2015GL063652

Hansen, J., Ruedy, R., Sato, M., & Lo, K. (2010). Global surface temperature change. *Reviews of Geophysics*, *48*, RG4004. https://doi.org/10.1029/2010RG000345

Hart, R. E., Chavas, D. R., & Guishard, M. P. (2016). The arbitrary definition of the current Atlantic major hurricane landfall drought. *Bulletin of the American Meteorological Society*, *97*(5), 713–722. https://doi.org/10.1175/BAMS-D-15-00185.1

Hartmann, D. L., Klein Tank, A. M. G., Rusticucci, M., Alexander, L. V., Brönnimann, S., Charabi, Y. A. R., et al. (2013). Observations: Atmosphere and surface. Climate change 2013 the physical science basis: Working Group I contribution to the fifth assessment report of the intergovernmental panel on climate change, 9781107057, 159–254. https://doi.org/10.1017/CBO9781107415324.008

Held, I. M., & Soden, B. J. (2006). Robust responses of the hydrological cycle to global warming. *Journal of Climate*, *19*(21), 5686–5699. https://doi.org/10.1175/JCLI3990.1

Hernández Ayala, J. J., & Matyas, C. J. (2016). Tropical cyclone rainfall over Puerto Rico and its relations to environmental and storm-specific factors. *International Journal of Climatology*, *36*(5), 2223–2237. https://doi.org/10.1002/joc.4490

Holm, S. (1979). A simple sequentially rejective multiple test procedure. *Scandinavian Journal of Statistics*, *6*(2), 65–70. Retrieved from https://www.jstor.org/stable/4615733

Jarvinen, B. R., Neumann, C. J., & Davis, M. A. S. (1984). A tropical cyclone data tape for the North Atlantic basin, 1886–1983: Contents, limitations, and uses. NOAA Tech. Memo NWS NHC 22, NOAA/Tropical Prediction Center. NOAA Tech. Memo NWS NHC 22, NOAA/Tropical Prediction Center, Miami, Fla.

Jiang, H., Halverson, J. B., Simpson, J., & Zipser, E. J. (2008). Hurricane "rainfall potential" derived from satellite observations aids overland rainfall prediction. *Journal of Applied Meteorology and Climatology*, *47*(4), 944–959. https://doi.org/10.1175/2007JAMC1619.1

Jonkman, S. N., Godfroy, M., Sebastian, A., & Kolen, B. (2018). Brief communication: Loss of life due to Hurricane Harvey. *Natural Hazards and Earth System Sciences*, *18*(4), 1073–1078. https://doi.org/10.5194/nhess-18-1073-2018

Khouakhi, A., Villarini, G., & Vecchi, G. A. (2017). Contribution of tropical cyclones to rainfall at the global scale. *Journal of Climate*, *30*(1), 359–372. https://doi.org/10.1175/JCLI-D-16-0298.1

Kim, H. S., Vecchi, G. A., Knutson, T. R., Anderson, W. G., Delworth, T. L., Rosati, A., et al. (2014). Tropical cyclone simulation and response to CO2 doubling in the GFDL CM2.5 high-resolution coupled climate model. *Journal of Climate*, *27*(21), 8034–8054. https://doi.org/10.1175/JCLI-D-13-00475.1

Klotzbach, P. J., Schreck, C. J. III, Collins, J. M., Bell, M. M., Blake, E. S., & Roache, D. (2018). The extremely active 2017 North Atlantic hurricane season. *Monthly Weather Review*, *146*(10), 3425–3443. https://doi.org/10.1175/MWR-D-18-0078.1

Knaff, J. A., Longmore, S. P., & Molenar, D. A. (2014). An objective satellite-based tropical cyclone size climatology. *Journal of Climate*, *27*(1), 455–476. https://doi.org/10.1175/JCLI-D-13-00096.1

Knutson, T., Camargo, S. J., Chan, J. C. L., Emanuel, K., Ho, C.-H., Kossin, J., et al. (2018). Tropical cyclones and climate change assessment: Part I. Detection and attribution. *Bulletin of the American Meteorological Society*, *100*(10), 1987–2007. https://doi.org/10.1175/BAMS-D-18-0189.1

Knutson, T. R., McBride, J. L., Chan, J., Emanuel, K., Holland, G., Landsea, C., et al. (2010). Tropical cyclones and climate change. *Nature Geoscience*, *3*(3), 157–163. https://doi.org/10.1038/ngeo779

Knutson, T. R., Sirutis, J. J., Vecchi, G. A., Garner, S., Zhao, M., Kim, H. S., et al. (2013). Dynamical downscaling projections of twenty-first-century atlantic hurricane activity: CMIP3 and CMIP5 model-based scenarios. *Journal of Climate*, *26*(17), 6591–6617. https://doi.org/10.1175/JCLI-D-12-00539.1

Konrad, C. E., & Perry, L. B. (2009). Relationships between tropical cyclones and heavy rainfall in the Carolina region of the USA. *International Journal of Climatology*, *30*, n/a–534. https://doi.org/10.1002/joc.1894

Kossin, J. P., Emanuel, K. A., & Vecchi, G. A. (2014). The poleward migration of the location of tropical cyclone maximum intensity. *Nature*, *509*(7500), 349–352. https://doi.org/10.1038/nature13278

Kossin, J. P., Olander, T. L., & Knapp, K. R. (2013). Trend analysis with a new global record of tropical cyclone intensity. *Journal of Climate*, *26*(24), 9960–9976. https://doi.org/10.1175/JCLI-D-13-00262.1

Kossin, J. P., & Vimont, D. J. (2007). A more general framework for understanding atlantic hurricane variability and trends. *Bulletin of the American Meteorological Society*, *88*(11), 1767–1782. https://doi.org/10.1175/BAMS-88-11-1767

Kunkel, K. E., Easterling, D. R., Kristovich, D. A. R., Gleason, B., Stoecker, L., & Smith, R. (2010). Recent increases in U.S. heavy precipitation associated with tropical cyclones. *Geophysical Research Letters*, *37*, L24706. https://doi.org/10.1029/2010GL045164

Landsea, C. W., & Franklin, J. L. (2013). Atlantic hurricane database uncertainty and presentation of a new database format. *Monthly Weather Review*, *141*(10), 3576–3592. https://doi.org/10.1175/MWR-D-12-00254.1

Lau, W. K. M., & Zhou, Y. P. (2012). Observed recent trends in tropical cyclone rainfall over the North Atlantic and the North Pacific. *Journal of Geophysical Research*, *117*, D03104. https://doi.org/10.1029/2011JD016510

Lenssen, N. J. L., Schmidt, G. A., Hansen, J. E., Menne, M. J., Persin, A., Ruedy, R., & Zyss, D. (2019). Improvements in the uncertainty model in the Goddard Institute for Space Studies Surface Temperature (GISTEMP) analysis. *Journal of Geophysical Research: Atmospheres*, *124*, 6307–6326. https://doi.org/10.1029/2018JD029522

Liu, M., & Smith, J. A. (2016). Extreme rainfall from landfalling tropical cyclones in the eastern United States: Hurricane Irene (2011). *Journal of Hydrometeorology*, *17*(11), 2883–2904. https://doi.org/10.1175/JHM-D-16-0072.1

Liu, M., Vecchi, G. A., Smith, J. A., & Murakami, H. (2018). Projection of landfalling-tropical cyclone rainfall in the eastern United States under anthropogenic warming. *Journal of Climate*, *31*(18), 7269–7286. https://doi.org/10.1175/JCLI-D-17-0747.1

Matyas, C. J. (2010). Associations between the size of hurricane rain fields at landfall and their surrounding environments. *Meteorology and Atmospheric Physics*, *106*(3–4), 135–148. https://doi.org/10.1007/s00703-009-0056-1

Menne, M. J., Durre, I., Vose, R. S., Gleason, B. E., & Houston, T. G. (2012). An overview of the global historical climatology network-daily database. *Journal of Atmospheric and Oceanic Technology*, *29*(7), 897–910. https://doi.org/10.1175/JTECH-D-11-00103.1

National Centers for Environmental Prediction. (2001). Tropical Storm Allison—June 4-18, 2001. Retrieved June 2, 2019, from https://www.wpc.ncep.noaa.gov/tropical/rain/allison2001.html

NOAA National Centers for Environmental Information (NCEI) (2019) U.S. billion-dollar weather and climate disasters. Retrieved from https://www.ncdc.noaa.gov/billions/

Patricola, C. M., Saravanan, R., & Chang, P. (2014). The impact of the El Niño-Southern oscillation and Atlantic meridional mode on seasonal Atlantic tropical cyclone activity. *Journal of Climate*, *27*(14), 5311–5328. https://doi.org/10.1175/JCLI-D-13-00687.1

Patricola, C. M., & Wehner, M. F. (2018). Anthropogenic influences on major tropical cyclone events. *Nature*, *563*(7731), 339–346. https://doi.org/10.1038/s41586-018-0673-2

Prat, O. P., & Nelson, B. R. (2016). On the link between tropical cyclones and daily rainfall extremes derived from global satellite observations. *Journal of Climate*, *29*(17), 6127–6135. https://doi.org/10.1175/JCLI-D-16-0289.1

Rappaport, E. N. (2000). Loss of life in the United States associated with recent atlantic tropical cyclones. *Bulletin of the American Meteorological Society*, *81*(9), 2065–2073. https://doi.org/10.1175/1520-0477(2000)081<2065:LOLITU>2.3.CO;2

Rappaport, E. N. (2013). Fatalities in the United States from Atlantic tropical cyclones: New data and interpretation. *Bulletin of the American Meteorological Society*, *95*(3), 341–346. https://doi.org/10.1175/bams-d-12-00074.1

Risser, M. D., & Wehner, M. F. (2017). Attributable human-induced changes in the likelihood and magnitude of the observed extreme precipitation during hurricane Harvey. *Geophysical Research Letters*, *44*, 12,457–12,464. https://doi.org/10.1002/2017GL075888

Ross, R. J., & Elliot, W. P. (1996). Tropospheric water vapor climatology and trends over North America: 1973-93. *Journal of Climate*, *9*, 3561–3574.

Schott, T., Landsea, C. W., Hafele, G., Lorens, J., Thurm, H., Ward, B., et al. (2012). The Saffir-Simpson Hurricane Wind Scale. National Hurricane Center. Retrieved from http://www.nhc.noaa.gov/pdf/sshws.pdf

Scoccimarro, E., Gualdi, S., Villarini, G., Vecchi, G. A., Zhao, M., Walsh, K., & Navarra, A. (2014). Intense precipitation events associated with landfalling tropical cyclones in response to a warmer climate and increased CO2. *Journal of Climate*, *27*(12), 4642–4654. https://doi.org/10.1175/JCLI-D-14-00065.1

Sheskin, D. J. (2003). *Handbook of parametric and nonparametric statistical procedures (third)*. New York: Chapman and Hall/CRC. https://doi.org/10.1201/9781420036268

Simpson, A. G. (2018). FEMA expands flood reinsurance program with private reinsurers for 2018.

Skok, G., Bacmeister, J., & Tribbia, J. (2013). Analysis of tropical cyclone precipitation using an object-based algorithm. *Journal of Climate*, *26*(8), 2563–2579. https://doi.org/10.1175/JCLI-D-12-00135.1

Sobel, A. H., Camargo, S. J., Hall, T. M., Lee, C., Tippett, M. K., & Wing, A. A. (2016). Human influence on tropical cyclone intensity. *Science*, *353*(6296), 242–246. https://doi.org/10.1126/science.aaf6574

Team, G. (2019). GISS surface temperature analysis (GISTEMP), version 4. https://doi.org/https://data.giss.nasa.gov/gistemp/

Touma, D., Michalak, A. M., Swain, D. L., & Diffenbaugh, N. S. (2018). Characterizing the spatial scales of extreme daily precipitation in the United States. *Journal of Climate*, *31*(19), 8023–8037. https://doi.org/10.1175/JCLI-D-18-0019.1

Trenberth, K. E., Dai, A., Rasmussen, R. M., & Parsons, D. B. (2003). The changing character of precipitation. *Bulletin of the American Meteorological Society*, *84*(9), 1205–1218. https://doi.org/10.1175/BAMS-84-9-1205

Trenberth, K. E., Fasullo, J., & Smith, L. (2005). Trends and variability in column-integrated atmospheric water vapor. *Climate Dynamics*, *24*, 741–758. https://doi.org/10.1007/s00382-005-0017-4

Truchelut, R. E., & Staehling, E. M. (2017). An energetic perspective on United States tropical cyclone landfall droughts. *Geophysical Research Letters*, *44*, 12,013–12,019. https://doi.org/10.1002/2017GL076071

Upton, L., Kirsch, T. D., Harvey, M., & Hanfling, D. (2017). Health care coalitions as response organizations: Houston after Hurricane Harvey. *Disaster Medicine and Public Health Preparedness*, *11*(6), 637–639. https://doi.org/10.1017/dmp.2017.141

van Oldenborgh, G. J., van der Wiel, K., Sebastian, A., Singh, R., Arrighi, J., Otto, F., et al. (2017). Attribution of extreme rainfall from Hurricane Harvey, August 2017. *Environmental Research Letters*, *12*(12), 124009. https://doi.org/10.1088/1748-9326/aa9ef2

Villarini, G., Lavers, D. A., Scoccimarro, E., Zhao, M., Wehner, M. F., Vecchi, G. A., et al. (2014). Sensitivity of tropical cyclone rainfall to idealized global-scale forcings. *Journal of Climate*, *27*(12), 4622–4641. https://doi.org/10.1175/JCLI-D-13-00780.1

Villarini, G., Smith, J. A., Baeck, M. L., Marchok, T., & Vecchi, G. A. (2011). Characterization of rainfall distribution and flooding associated with U.S. landfalling tropical cyclones: Analyses of Hurricanes Frances, Ivan, and Jeanne (2004). *Journal of Geophysical Research*, *116*, D23116. https://doi.org/10.1029/2011JD016175

Villarini, G., Smith, J. A., Vitolo, R., & Stephenson, D. B. (2013). On the temporal clustering of US floods and its relationship to climate teleconnection patterns. *International Journal of Climatology*, *33*(3), 629–640. https://doi.org/10.1002/joc.3458

Vose, R. S., Arndt, D., Banzon, V. F., Easterling, D. R., Gleason, B., Huang, B., et al. (2012). NOAA's merged land-ocean surface temperature analysis. *Bulletin of the American Meteorological Society*, *93*(11), 1677–1685. https://doi.org/10.1175/BAMS-D-11-00241.1

Walsh, K. J. E., McBride, J. L., Klotzbach, P. J., Balachandran, S., Camargo, S. J., Holland, G., et al. (2016). Tropical cyclones and climate change. *Wiley Interdisciplinary Reviews: Climate Change*, *7*(1), 65–89. https://doi.org/10.1002/wcc.371

Wang, S.-Y. S., Zhao, L., Yoon, J.-H., Klotzbach, P., & Gillies, R. R. (2018). Quantitative attribution of climate effects on Hurricane Harvey's extreme rainfall in Texas. *Environmental Research Letters*, *13*, 1–10. https://doi.org/10.1088/1748-9326/aabb85

Wright, D. B., Knutson, T. R., & Smith, J. A. (2015). Regional climate model projections of rainfall from U.S. landfalling tropical cyclones. *Climate Dynamics*, *45*(11-12), 3365–3379. https://doi.org/10.1007/s00382-015-2544-y

Yeo, C. J. J., Román, G. C., Kusnerik, D., Burt, T., Mersinger, D., Thomas, S., et al. (2018). Trainee responses to Hurricane Harvey: Correlating volunteerism with burnout. *Frontiers in Public Health*, *6*(August), 1–8. https://doi.org/10.3389/fpubh.2018.00224

Yu, C.-K., & Cheng, L.-W. (2013). Distribution and mechanisms of orographic precipitation associated with Typhoon Morakot (2009). *Journal of the Atmospheric Sciences*, *70*(9), 2894–2915. https://doi.org/10.1175/JAS-D-12-0340.1

Zhang, W., Villarini, G., Vecchi, G. A., & Smith, J. A. (2018). Urbanization exacerbated the rainfall and flooding caused by hurricane Harvey in Houston. *Nature*, *563*(7731), 384–388. https://doi.org/10.1038/s41586-018-0676-z

Zhou, Y., & Matyas, C. J. (2017). Spatial characteristics of storm-total rainfall swaths associated with tropical cyclones over the Eastern United States. *International Journal of Climatology*, *37*(February), 557–569. https://doi.org/10.1002/joc.5021

Zhu, L., & Quiring, S. M. (2013). Variations in tropical cyclone precipitation in Texas (1950 to 2009). *Journal of Geophysical Research: Atmospheres*, *118*, 3085–3096. https://doi.org/10.1029/2012JD018554

Zick, S. E., & Matyas, C. J. (2016). Precipitation patterns in tropical cyclones. *Annals of the American Association of Geographers*, *106*, 1217–1235.